

Shock Wave Compression of Benzene, Carbon Disulfide, Carbon Tetrachloride, and Liquid Nitrogen*†

RICHARD D. DICK

DICK-RD 70-0211

Los Alamos Scientific Laboratory, Los Alamos, New Mexico 87544

(Received 22 August 1969)

Hugoniot data to several hundred kilobar have been obtained for benzene, carbon disulfide, carbon tetrachloride, and liquid nitrogen. Standard high explosive techniques were used for generating the shock waves. Experimentally measured quantities were transformed to pressure and volume data by the impedance match method. The shock-particle velocity data for the liquids are described by a linear relationship, however, a quadratic in particle velocity also provides an adequate representation of the data for carbon tetrachloride and liquid nitrogen. Benzene undergoes a transition at 133 kbar and carbon disulfide at 62 kbar. These transitions are accompanied by a volume decrease of approximately 16%. A double shock-wave structure, observed in many solids which undergo a transition, was not observed in benzene and carbon disulfide. There is some evidence that carbon tetrachloride and liquid nitrogen undergo a transition at 165 and 135 kbar, respectively. Hugoniot curves calculated from a Lennard-Jones and Devonshire (6-9) and a modified Buckingham exp-6 intermolecular potential fit the liquid nitrogen experimental Hugoniot curve between 20 and 170 kbar.

I. INTRODUCTION

These are the results of an investigation to determine some of the properties of benzene, carbon disulfide, carbon tetrachloride, and liquid nitrogen when shocked to pressures of several hundred kilobars. The pressures were produced by plane shock waves, created by detonating high explosives. The initial temperature of the three organic liquids was approximately 295°K and of the liquid nitrogen 75°K.

There is very little high-pressure data available on these liquids. Bridgman¹⁻⁷ has obtained most of the static pressure data. A limited amount of shock compression data were obtained by Walsh and Rice⁸ for benzene, carbon disulfide, and carbon tetrachloride, using optical techniques. More extensive dynamic data for these liquids were collected by Cook and Rogers,⁹ also using optical methods. Zubarev and Telegin¹⁰ obtained some Hugoniot data for liquid nitrogen using techniques similar to those of this investigation.

The "impedance match method" was used to transform the measured shock velocities to pressure, particle velocity, and relative volume data. These data are presented in shock velocity-versus-particle velocity and pressure-versus-relative volume plots. In addition some rough electrical conductivity experiments were carried out on benzene, carbon disulfide, and carbon tetrachloride. The discovery that benzene and carbon disulfide undergo a transition prompted experiments to detect the presence of a double shock-wave structure associated with the transition; the results were negative.

II. EXPERIMENTAL TECHNIQUE

The impedance match method, as used in this study, requires the measurement of the shock velocity and the initial density of the material being examined and the shock velocity in a standard to determine the Hugoniot data. In this investigation 2024 dural

was used as the standard. The Rankine-Hugoniot relations¹¹⁻¹³

$$P - P_0 = \rho_0 U_s U_p, \quad (1)$$

$$V/V_0 = (U_s - U_p)/U_s, \quad (2)$$

for conservation of momentum and mass across the shock front provide the connection between the measured quantities and the Hugoniot point for the unknown material. The pressure and particle velocity

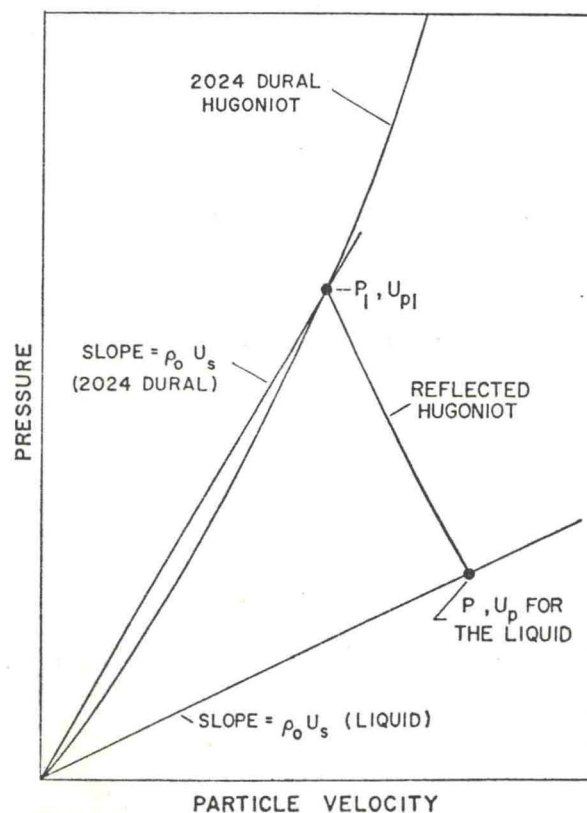


Fig. 1. Graphic representation of the impedance match method.

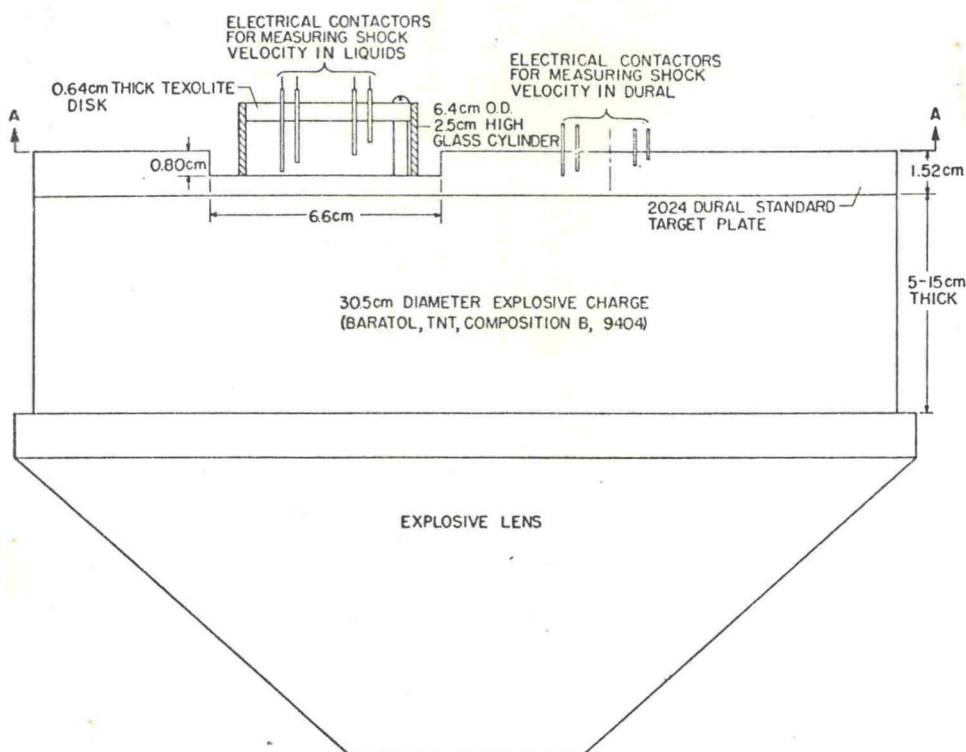


FIG. 2. Cross-sectional view of the shot assembly used for the organic liquids.

must be continuous across the interface between the standard and the material under study. In the above equations P_0 and $V_0 (=1/\rho_0)$ represent the pressure and specific volume ahead of the shock front and P and V the pressure and specific volume behind the shock front. U_s and U_p represent the shock velocity and particle velocity relative to the undisturbed material ahead of the shock front. V/V_0 is defined as the relative volume. The curves in the $P-U_p$ plane in Fig. 1 illustrate the impedance match method. The measurement of the shock velocity in the known 2024 dural determines the state P_1, U_{p1} . From this point the reflected Hugoniot curve is constructed and intersects the line of slope $\rho_0 U_s$ determined for the liquid. This intersection is the pressure and particle velocity (P, U_p) in the sample.

The Hugoniot for the 2024 dural has been measured very accurately at ambient temperature. The equation of state¹⁴ is expressed by

$$U_s = 5.328 + 1.338U_p \quad (3)$$

with $\rho_0 = 2.785$ g/cc and the Gruneisen ratio $\Gamma_0 = 2.0$.

A detailed description of the experimental apparatus and fabricating techniques are given in Ref. 15. A cross-sectional view of the experimental apparatus used for the organic liquids is presented in Fig. 2. Three liquids were examined in a single experiment. Each liquid was contained in a glass cylinder set into a well machined in the target plate. The shock ve-

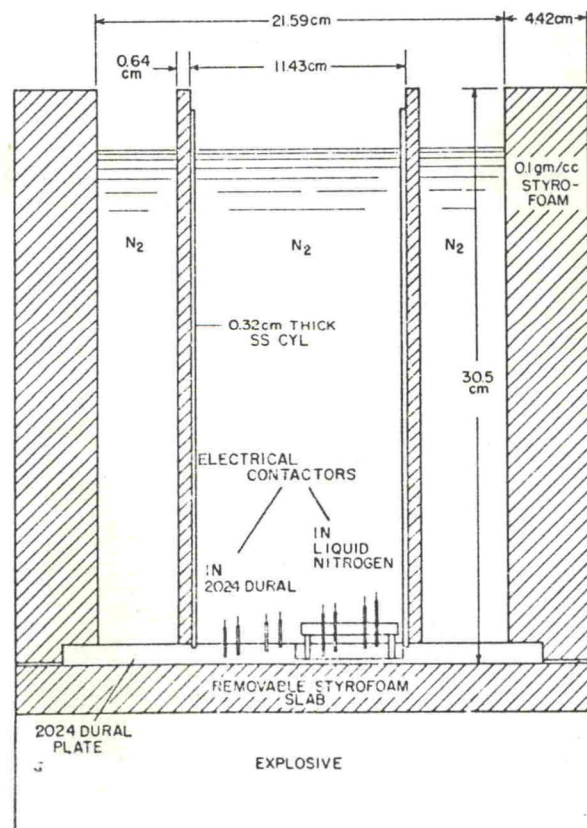


FIG. 3. Cross section view of the apparatus used for the liquid nitrogen.

TABLE I. Shock wave data for benzene.

Initial density (g/cc)	Shock velocity (km/sec)	Particle velocity (km/sec)	Pressure (kbar)	Relative volume (V/V_0)	Dural shock velocity (km/sec)
0.877	2.78±0.01	0.77±0.09	19±2	0.722±0.031	5.93±0.07
0.869	2.72±0.01	0.89±0.04	21±1	0.671±0.016	6.02±0.03
0.870	2.96±0.02	0.89±0.05	23±1	0.700±0.016	6.02±0.04
0.870	3.31±0.01	1.05±0.03	30±1	0.684±0.009	6.16±0.02
0.875	3.44±0.01	1.12±0.03	34±1	0.676±0.009	6.22±0.03
0.879	3.47±0.01	1.12±0.04	34±1	0.676±0.011	6.23±0.03
0.880	3.85±0.01	1.36±0.03	46±1	0.647±0.008	6.43±0.02
0.866	3.89±0.00	1.45±0.02	49±1	0.627±0.006	6.50±0.02
0.885	4.05±0.01	1.45±0.03	52±1	0.642±0.007	6.52±0.02
0.877	4.05±0.01	1.48±0.03	53±1	0.635±0.006	6.54±0.02
0.881	4.09±0.01	1.59±0.09	57±3	0.612±0.021	6.62±0.07
0.869	4.38±0.01	1.77±0.03	67±1	0.597±0.006	6.78±0.02
0.869	4.52±0.01	1.85±0.01	73±1	0.591±0.003	6.86±0.01
0.885	4.79±0.02	1.90±0.05	81±2	0.603±0.010	6.92±0.04
0.871	4.77±0.02	1.94±0.02	81±1	0.593±0.004	6.95±0.02
0.870	5.00±0.02	2.16±0.10	94±4	0.567±0.019	7.14±0.08
0.870	5.28±0.01	2.29±0.02	105±1	0.567±0.003	7.26±0.01
0.875	5.46±0.01	2.33±0.02	111±1	0.575±0.004	7.31±0.02
0.880	5.52±0.02	2.37±0.04	115±2	0.570±0.007	7.35±0.03
0.868	5.71±0.01	2.61±0.03	129±2	0.542±0.005	7.56±0.03
0.887	6.00±0.03	2.86±0.03	152±2	0.523±0.006	7.80±0.03
0.871	5.93±0.02	2.92±0.02	151±1	0.507±0.004	7.83±0.02
0.876	6.17±0.02	3.34±0.08	180±4	0.458±0.013	8.20±0.06
0.870	6.22±0.04	3.44±0.06	186±3	0.446±0.010	8.29±0.05
0.870	6.43±0.03	3.66±0.03	205±2	0.430±0.005	8.48±0.03
0.874	6.82±0.06	3.92±0.09	234±6	0.425±0.015	8.74±0.08
0.881	7.23±0.01	4.15±0.04	264±3	0.426±0.006	8.97±0.04
0.872	7.16±0.03	4.20±0.07	262±5	0.413±0.011	9.00±0.06
0.871	7.25±0.03	4.29±0.09	271±6	0.409±0.013	9.08±0.08
0.875	7.66±0.05	4.61±0.06	309±4	0.398±0.009	9.39±0.05
0.876	8.24±0.05	4.99±0.07	360±5	0.395±0.009	9.77±0.06
0.876	8.61±0.04	5.21±0.07	393±6	0.395±0.009	10.00±0.06
0.881	8.91±0.07	5.38±0.14	422±12	0.396±0.017	10.17±0.12
0.871	8.82±0.08	5.42±0.12	416±10	0.386±0.015	10.18±0.10
0.874	8.97±0.06	5.51±0.11	432±9	0.386±0.013	10.28±0.09

locities in the liquids were determined from the times at which the shock front arrives at the coaxial electrical contactors¹⁶ located in the liquids at accurately measured distances from the 2024 dural plate-liquid interface. Other electrical contactors are placed in holes of accurately measured depths in the 2024 dural plate to determine the arrival time of the shock front at these levels. The shock velocity in each material was computed from a plot of the corresponding time-distance data.

The methods and techniques used for the liquid nitrogen experiments are similar. Figure 3 is a diagram of the shot assembly showing the double-walled construction for keeping the liquid nitrogen in a non-boiling state. A few seconds before detonating the explosive the styrofoam slab was removed remotely. This ensures that the cold apparatus is in contact with the warm explosive for a minimal period of time.

The observation of a transition occurring in benzene

and carbon disulfide and the character of their U_s-U_p plots led to some experiments to determine if a double shock wave structure^{17,18} was present. The apparatus consisted of a 2024 dural driver plate 0.64 cm thick backed by the appropriate explosive system, a liquid layer 1.27 or 2.54 cm thick, and a 0.64 cm thick 2024 dural cover plate. The free surface motion of the cover plate was determined from the times at which the electrical contactor pins positioned above the plate are shorted. If at the transition pressure the original shock wave is unstable two shock waves with different velocities are formed, one with the pressure of the transition and the other with the remainder of the pressure pulse. A separation in time occurs as the two shock waves traverse the liquid layer and cover plate. By doubling the thickness of the liquid the time separation is also doubled, neglecting attenuation. The free surface motion of the cover plate results from the two impulses received from the two shock waves. Care was

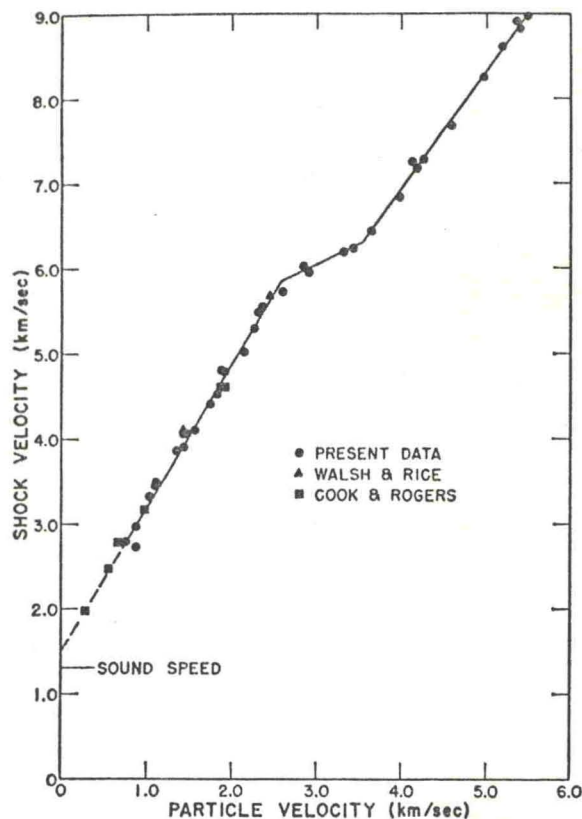


FIG. 4. Shock velocity-versus-particle velocity plot for benzene.

taken in designing the experiment to see that extraneous shock waves were not present.

III. EXPERIMENTAL RESULTS AND INTERPRETATION

A. General

The data for each liquid are presented as U_s-U_p and $P-V/V_0$ graphs. A linear relationship between U_s and U_p was observed for each of the liquids. The data were fit by a linear least-squares method to the equation

$$U_s = C + SU_p \quad (4)$$

The carbon tetrachloride and liquid nitrogen U_s-U_p data were also fit to a quadratic in U_p ,

$$U_s = C + SU_p + TU_p^2 \quad (5)$$

Benzene and carbon disulfide undergo a transition. There is less convincing evidence for the occurrence of a transition in carbon tetrachloride and liquid nitrogen.

For all materials the errors associated with the measured shock velocities represent the standard deviations computed from the linear least-squares fit of the time-distance data. These data were initially corrected for tilt in the shock wave. The standard deviations listed with the calculated values for pressure,

particle velocity, and relative volume were determined from the standard deviations computed for the measured shock velocities. The precision of the pin setback and hole depth measurements was 5μ and the precision in reading the pin signal times was 5 nsec. There was negligible attenuation of the shock wave over the distance established for measuring the shock velocity. The liquid density errors were about $\frac{1}{3}\%$ due mainly to a 2°C error in the temperature measurement.

The three organic liquids were reagent grade with a purity better than 99%. The liquid nitrogen was about 99% pure with the major impurity being oxygen.

B. Benzene

The Hugoniot data for benzene are listed in Table I. The U_s-U_p plot shown in Fig. 4 shows three line segments representing the data. An interesting feature of this graph is the short middle segment which has a relatively small slope. There is good agreement with the data of Walsh and Rice⁸ and Cook and Rogers.⁹ In the interval $2.70 \leq U_s \leq 5.83$ km/sec the fit of the U_s-U_p points is

$$U_s = 1.50 \pm 0.10 + (1.67 \pm 0.04) U_p \quad (6)$$

and from $6.26 \leq U_s \leq 9.00$ km/sec

$$U_s = 1.37 \pm 0.17 + (1.39 \pm 0.03) U_p \quad (7)$$

The short segment between $U_s = 5.83$ and 6.26 km/sec is fit by

$$U_s = 4.64 \pm 0.99 + (0.46 \pm 0.10) U_p \quad (8)$$

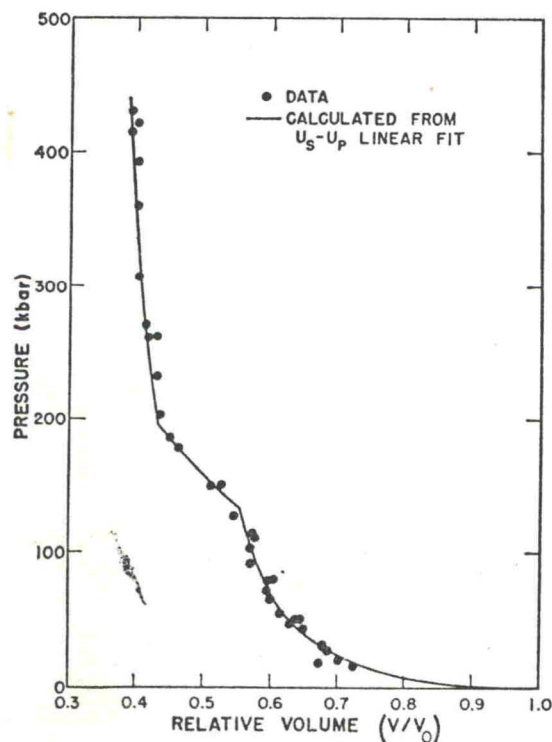


FIG. 5. Pressure-versus-relative volume plot for benzene.

TABLE II. Shock wave data for carbon disulfide.

Initial density (g/cc)	Shock velocity (km/sec)	Particle velocity (km/sec)	Pressure (kbar)	Relative volume (V/V_0)	Dural shock velocity (km/sec)
1.260	2.47±0.01	0.75±0.08	23±3	0.698±0.033	5.93±0.07
1.249	2.41±0.00	0.86±0.04	26±1	0.642±0.017	6.02±0.03
1.251	2.59±0.01	0.86±0.05	28±2	0.668±0.017	6.02±0.04
1.251	2.94±0.01	1.01±0.03	37±1	0.658±0.010	6.16±0.02
1.257	3.06±0.01	1.07±0.03	41±1	0.650±0.010	6.22±0.03
1.263	3.09±0.01	1.08±0.04	42±2	0.651±0.012	6.23±0.03
1.264	3.39±0.01	1.31±0.03	56±1	0.615±0.008	6.43±0.02
1.245	3.43±0.01	1.39±0.02	59±1	0.594±0.006	6.50±0.02
1.272	3.47±0.01	1.40±0.03	62±1	0.597±0.008	6.52±0.02
1.260	3.47±0.01	1.42±0.02	62±1	0.590±0.007	6.54±0.02
1.266	3.51±0.01	1.52±0.08	68±4	0.566±0.024	6.62±0.07
1.249	3.53±0.01	1.72±0.02	76±1	0.513±0.007	6.78±0.02
1.249	3.55±0.01	1.81±0.01	80±1	0.491±0.004	6.86±0.01
1.272	3.65±0.01	1.87±0.05	87±2	0.489±0.013	6.92±0.04
1.253	3.62±0.01	1.91±0.02	87±1	0.473±0.006	6.95±0.02
1.251	3.78±0.01	2.13±0.09	101±5	0.436±0.025	7.14±0.08
1.251	4.02±0.01	2.25±0.02	113±1	0.442±0.004	7.26±0.01
1.257	4.18±0.00	2.28±0.02	120±1	0.454±0.004	7.31±0.02
1.264	4.20±0.01	2.33±0.04	124±2	0.446±0.009	7.35±0.03
1.248	4.40±0.01	2.56±0.03	141±2	0.420±0.007	7.56±0.03
1.275	4.86±0.02	2.77±0.03	172±2	0.430±0.006	7.80±0.03
1.253	4.80±0.01	2.83±0.02	170±1	0.410±0.005	7.83±0.02
1.258	5.23±0.02	3.20±0.08	211±5	0.388±0.015	8.20±0.06
1.251	5.20±0.02	3.31±0.06	215±4	0.364±0.011	8.29±0.05
1.251	5.68±0.03	3.48±0.03	247±2	0.388±0.006	8.48±0.03
1.255	6.04±0.03	3.72±0.09	282±7	0.384±0.015	8.74±0.08
1.266	6.46±0.02	3.92±0.04	320±4	0.396±0.007	8.97±0.04
1.254	6.36±0.02	3.98±0.07	317±6	0.375±0.011	9.00±0.06
1.253	6.44±0.04	4.06±0.09	328±7	0.371±0.014	9.08±0.08
1.257	6.73±0.03	4.37±0.06	370±5	0.351±0.010	9.39±0.05
1.258	7.34±0.04	4.71±0.07	435±6	0.358±0.010	9.77±0.06
1.258	7.64±0.05	4.93±0.07	473±7	0.355±0.010	10.00±0.06
1.266	7.84±0.03	5.09±0.14	504±14	0.350±0.018	10.17±0.12
1.253	7.98±0.08	5.09±0.12	509±12	0.363±0.017	10.18±0.10
1.255	8.09±0.05	5.18±0.11	526±11	0.360±0.014	10.28±0.09

Included on the graph is the measured sound speed¹⁹ of the liquid benzene at 22°C and local atmospheric pressure. In Fig. 5 the $P-V/V_0$ data are plotted along with the curves transformed from the fit of the U_s-U_p data. The initial density was 0.879 g/cc.

The U_s-U_p and $P-V/V_0$ plots indicate that a transition begins at about $U_s=5.80$ and $U_p=2.60$ km/sec, and a pressure of 133 kbar, and ends at about $U_s=6.30$, $U_p=3.50$, and a pressure of 194 kbar. It is possible that a transition occurs below 5 kbar since the lowest line segment extrapolates to a value on the U_s axis 14% higher than the measured sound speed. The $P-V/V_0$ data of Fig. 5 are represented by concave upward curves below 133 kbar and above 194 kbar, with a third curve fitted to the few points in between. If the upper Hugoniot curve is extrapolated to 133 kbar and the lower Hugoniot curve is used as a reference, the change in V/V_0 due to the transition is about 16%.

In many solids the occurrence of a normal instantaneous (less than 0.1 μ sec) transition is represented in the U_s-U_p plane by either a change in slope or by an interval of constant shock velocity. The latter case is usually accompanied by a double shock wave structure. The benzene U_s-U_p plot appears to contain a combination of both characteristics since the shock velocity increases very slowly with particle velocity over the small interval described in Eq. (8). However, the formation of a double shock structure is not expected because the Rayleigh line from the foot of the $P-V/V_0$ curve connects all points on the Hugoniot in a single shock process. This conclusion was verified by the performance of some double shock wave experiments as explained in Sec. II. Based on the above observations and a knowledge of other materials,^{18,20} benzene is believed to undergo an instantaneous transition for two reasons: (1) a sluggish (greater than 1 μ sec) transition is unlikely because a plot of the U_s-U_p data shows a

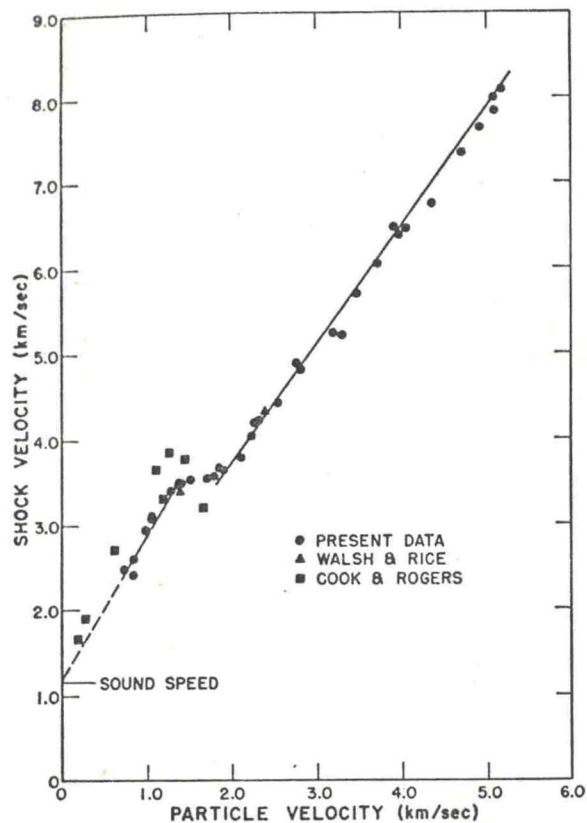


FIG. 6. Shock velocity-versus-particle velocity plot for carbon disulfide.

discontinuous change in slope and (2) there was negligible attenuation of the shock wave, indicating that a time dependent transition with a relaxation time of the order of the velocity measuring time does not occur. The absence of a double shock wave structure indicates the shock wave at the transition pressure is stable. Hence, the 133–194 kbar region may be a mixed phase region that occurs when a portion of the benzene transforms immediately to a new phase. The transformation is then complete at 194 kbar.

It is doubtful that the transition is due to freezing because the duration of the shock process is too short for rearrangement of the benzene molecules into a specific solid structure. Furthermore, pressure hinders rotation of the molecules. A temperature calculated at the beginning of the transition is 2300°K, based on the Mie-Grüneisen form¹⁵ for the equation of state. Under these extreme conditions of pressure and temperature, the molecular bonds are distorted sufficiently that polymerization can occur. Above 194 kbar the entire volume has undergone the transition and the Hugoniot curve is that of a more compact material. The temperature at this pressure is probably above 3500°K. A dynamic high-pressure study²¹ of some solid aromatic hydrocarbons (anthracene, pyrene, and phenanthrene) indicated that their behavior was similar to that of benzene. It was found that anthracene

transformed at about 180 kbar, phenanthrene at about 200 kbar, and pyrene at about 240 kbar. Hence, the transition pressures of the aromatic hydrocarbons and benzene are arranged according to the complexity of the individual molecules with benzene at the lowest and pyrene at the highest pressure. Perhaps benzene and the solid aromatic hydrocarbons undergo similar transformations.

The results of electrical conductivity experiments performed on benzene indicate no appreciable increase in conductivity up to pressures of 140 kbar.

The Hugoniot curve calculated by Salzman, Collings, and Pings²² using a Lennard-Jones and Devonshire intermolecular potential form appears to agree with the experimental Hugoniot curve up to about 130 kbar. The parameters they computed are $n=6.9$ (repulsion term), $r^*=5.92 \text{ \AA}$ (position of the potential minimum), and $T^*=440^\circ\text{K}$ (temperature equivalent of the potential minimum).

C. Carbon Disulfide

The carbon disulfide Hugoniot data are presented numerically in Table II and graphically in Figs. 6 and 7. Distinctive features of the U_s-U_p plot of Fig. 6 are the representation of the data by two line segments separated by an interval of constant shock

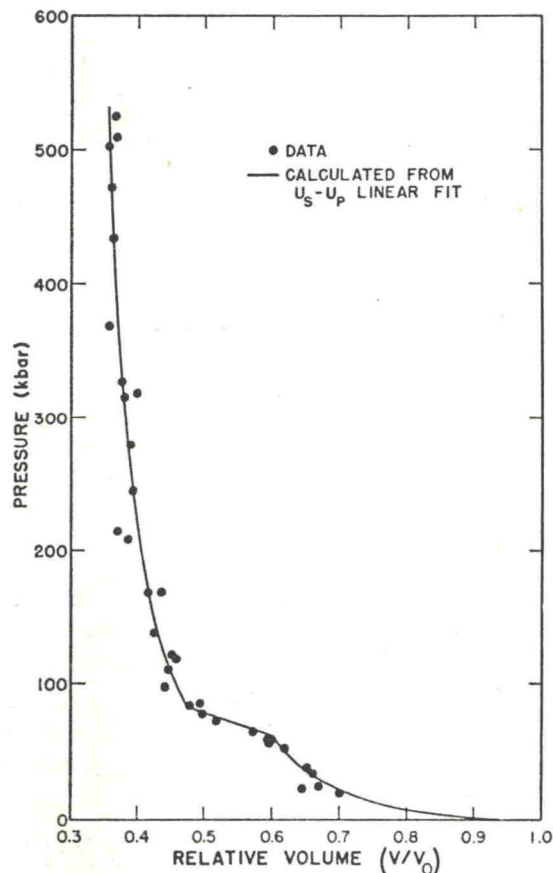


FIG. 7. Pressure-versus-relative volume plot for carbon disulfide.

TABLE III. Shock wave data for carbon tetrachloride.

Initial density (g/cc)	Shock velocity (km/sec)	Particle velocity (km/sec)	Pressure (kbar)	Relative volume (V/V_0)	Dural shock velocity (km/sec)
1.590	2.32±0.01	0.72±0.08	27±3	0.688±0.035	5.93±0.07
1.577	2.27±0.01	0.84±0.04	30±2	0.631±0.018	6.02±0.03
1.571	2.47±0.01	0.83±0.04	32±2	0.663±0.018	6.02±0.04
1.571	2.79±0.01	0.97±0.03	43±1	0.652±0.010	6.16±0.02
1.586	2.91±0.01	1.03±0.03	48±1	0.645±0.010	6.22±0.03
1.594	2.95±0.01	1.04±0.04	49±2	0.648±0.012	6.23±0.03
1.596	3.28±0.01	1.25±0.03	65±1	0.619±0.008	6.43±0.02
1.571	3.32±0.01	1.33±0.02	70±1	0.598±0.006	6.50±0.02
1.606	3.46±0.01	1.33±0.02	74±1	0.615±0.007	6.52±0.02
1.591	3.44±0.01	1.36±0.02	74±1	0.606±0.007	6.54±0.02
1.598	3.50±0.01	1.45±0.08	81±5	0.585±0.023	6.62±0.07
1.577	3.74±0.01	1.61±0.02	95±1	0.568±0.006	6.78±0.02
1.571	3.86±0.01	1.69±0.01	102±1	0.563±0.003	6.86±0.01
1.606	4.08±0.01	1.73±0.04	113±3	0.576±0.011	6.92±0.04
1.580	4.07±0.01	1.77±0.02	114±1	0.566±0.005	6.95±0.02
1.571	4.27±0.03	1.97±0.09	132±6	0.539±0.021	7.14±0.08
1.571	4.52±0.01	2.07±0.02	148±1	0.542±0.003	7.26±0.01
1.586	4.66±0.01	2.10±0.02	156±1	0.549±0.004	7.31±0.02
1.596	4.71±0.01	2.15±0.04	161±3	0.544±0.008	7.35±0.03
1.574	4.88±0.01	2.36±0.03	182±2	0.516±0.006	7.56±0.03
1.610	5.34±0.02	2.55±0.03	220±2	0.522±0.005	7.80±0.03
1.580	5.21±0.01	2.62±0.02	216±2	0.497±0.004	7.83±0.02
1.588	5.72±0.03	2.95±0.07	268±7	0.484±0.013	8.20±0.06
1.571	5.69±0.02	3.06±0.05	274±5	0.461±0.009	8.29±0.05
1.571	6.13±0.03	3.22±0.03	311±3	0.476±0.005	8.48±0.03
1.584	6.44±0.05	3.44±0.08	352±9	0.465±0.014	8.74±0.08
1.598	6.80±0.02	3.64±0.04	395±4	0.466±0.006	8.97±0.04
1.582	6.72±0.02	3.69±0.07	392±7	0.451±0.010	9.00±0.06
1.580	6.78±0.03	3.77±0.08	404±9	0.444±0.013	9.08±0.08
1.586	7.13±0.03	4.05±0.06	458±7	0.432±0.008	9.39±0.05
1.588	7.55±0.02	4.40±0.06	527±7	0.417±0.008	9.77±0.06
1.588	7.96±0.03	4.58±0.06	579±8	0.425±0.009	10.00±0.06
1.598	8.06±0.06	4.74±0.13	611±17	0.411±0.017	10.17±0.12
1.580	8.24±0.04	4.74±0.11	617±14	0.425±0.014	10.18±0.10
1.584	8.26±0.03	4.84±0.10	633±13	0.415±0.012	10.28±0.09

velocity and the excellent agreement between the measured sound speed¹⁹ and the intercept of the lower line with the U_s axis. The line segments were determined by a least-squares fit of the U_s-U_p data; in the region $2.40 \leq U_s \leq 3.50$ km/sec the relationship is

$$U_s = 1.18 \pm 0.22 + (1.67 \pm 0.14) U_p, \quad (9)$$

and from $3.50 \leq U_s \leq 8.20$ km/sec,

$$U_s = 1.11 \pm 0.07 + (1.35 \pm 0.02) U_p. \quad (10)$$

In the particle velocity interval of 1.39 to 1.84 km/sec, the shock velocity is essentially constant. The data of Walsh and Rice³ agree with the present data but those of Cook and Rogers⁹ do not. The abrupt change in the slope and the offset of the two line segments indicates a transition occurring at about 62 kbar ($U_s = 3.50$ km/sec, $U_p = 1.40$ km/sec, and $\rho_0 = 1.263$ g/cc) with a new phase formed at about 80 kbar

($U_s = 3.50$ km/sec, $U_p = 1.80$ km/sec, $\rho_0 = 1.263$ g/cc). The intercept of the lower line segment with the U_s axis (1.18 km/sec) is very close to the measured sound speed of 1.16 km/sec, indicating that carbon disulfide is in the liquid state from 1 bar–62 kbar.

The $P-V/V_0$ plot of Fig. 7 is characterized by concave upward curves above 80 kbar and below 62 kbar with a well-defined cusp representing the transition at 62 kbar. A straight line segment joins the two major curves. Using the lower curve as a reference, the decrease in relative volume ascribed to the transition is nearly 17%. Every point on the $P-V/V_0$ curves can be reached by the Rayleigh line in a single shock originating from the P_0, V_0 point. As a result there is no double shock wave structure associated with the transition even though an interval of constant shock velocity was observed in the U_s-U_p plot. This was confirmed by experiment (see Sec. II). The

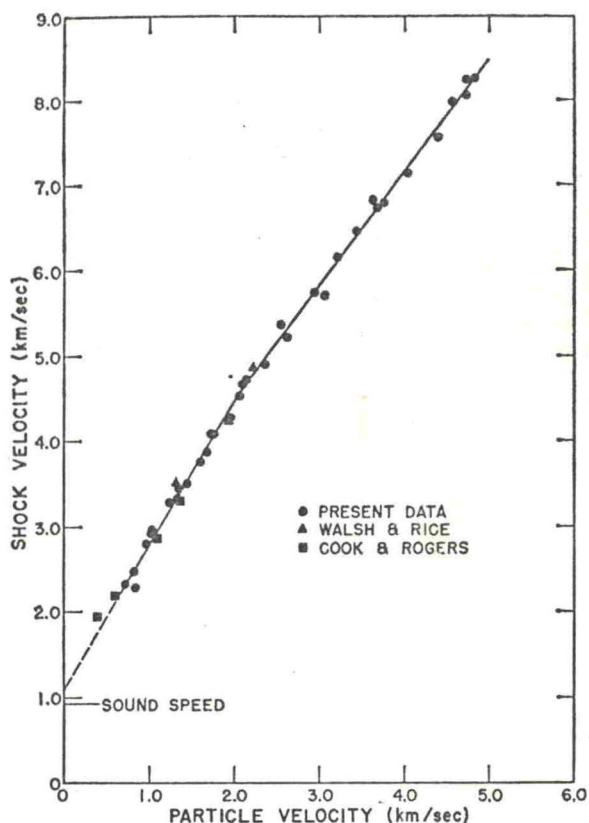


FIG. 8. Shock velocity-versus-particle velocity plot for carbon tetrachloride.

similarity in the observed behavior between carbon disulfide and benzene indicates that carbon disulfide undergoes an instantaneous transformation to a mixed phase material at 62 kbar with the new phase being completely formed at 80 kbar. In addition, the shock wave remains stable at and above the transition pressure.

The observed transition is thought to be a transformation from the liquid state to a "black substance" as observed by Bridgman.⁴ Whalley²³ and Butcher *et al.*²⁴ investigated the phenomenon and the transformed material in more detail. They found that under static pressures the transition takes place at about 40 kbar over a temperature range of 120–200°C. The black substance was determined to be an amorphous form of carbon disulfide, stable at ambient pressure and temperature, and has some of the characteristics of a semiconductor. In some experiments²⁵ where carbon disulfide was shocked to about 200 kbar, a black fluffy solid was recovered which may be the solid observed in the static experiments.

Some experiments were performed to determine the electrical properties of carbon disulfide near the transition pressure. It was observed, with rather insensitive instrumentation, that there was negligible electrical conductivity below the transition pressure. However, near 80 kbar the conductivity increased

significantly, indicating a connection between the transition and electrical conduction.

D. Carbon Tetrachloride

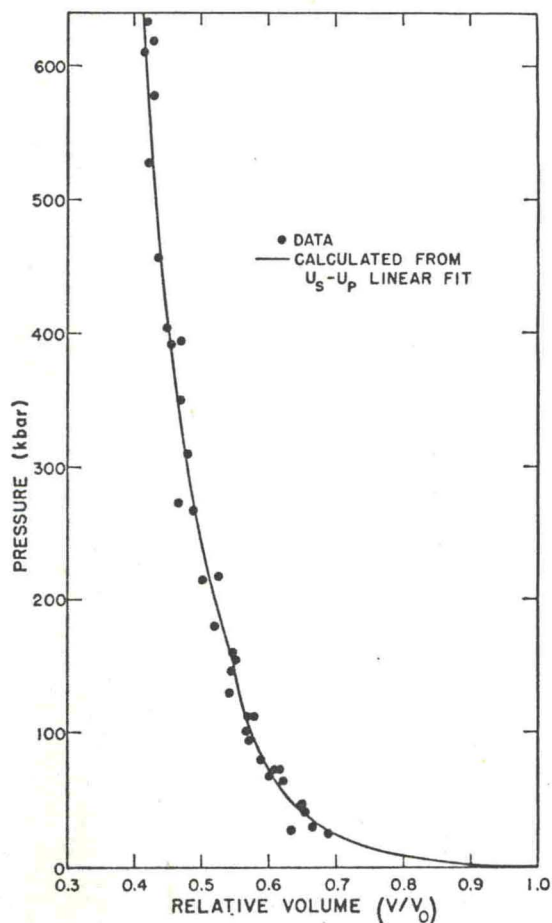
Carbon tetrachloride, in some respects, has a less complicated behavior under shock conditions than either benzene or carbon disulfide. In Table III are the Hugoniot data obtained from the experiments. The U_s-U_p data are plotted in Fig. 8 and are fit by two straight lines. They differ in slope, but there is no displacement of the two segments. The lines are fitted by

$$U_s = 1.11 \pm 0.08 + (1.67 \pm 0.05) U_p \quad (11)$$

in the range $2.30 \leq U_s \leq 4.70$ km/sec. Above $U_s = 4.70$ km/sec the linear relationship is

$$U_s = 1.87 \pm 0.14 + (1.32 \pm 0.03) U_p. \quad (12)$$

These lines intersect at $U_s = 4.70$ and $U_p = 2.17$ km/sec. A least-squares fit of the data to a quadratic in the particle velocity resulted in a smooth curve through



Pressure-versus-relative volume plot for carbon tetrachloride.

TABLE IV. Shock wave data for liquid nitrogen^a at 75°K.

Shock vel. (km/sec)	Particle vel. (km/sec)	Pressure (kbar)	Relative vol. (V/V_0)	Dural shock vel. (km/sec)
2.58±0.02	0.90±0.09	19±2	0.653±0.037	6.07±0.07
2.97±0.02	1.11±0.05	27±1	0.628±0.016	6.24±0.04
3.53±0.01	1.51±0.04	44±1	0.570±0.010	6.58±0.03
4.19±0.02	1.97±0.03	68±1	0.531±0.008	6.97±0.03
5.09±0.02	2.54±0.02	106±1	0.501±0.004	7.48±0.02
5.50±0.02	2.78±0.02	126±1	0.494±0.005	7.71±0.02
5.93±0.03	2.99±0.12	146±6	0.495±0.020	7.91±0.09
6.66±0.03	3.62±0.07	198±4	0.457±0.010	8.48±0.05
6.98±0.08	3.72±0.09	213±5	0.468±0.014	8.58±0.07
6.85±0.04	3.89±0.05	219±3	0.432±0.008	8.71±0.04
7.34±0.04	4.05±0.07	244±5	0.448±0.011	8.89±0.06
7.52±0.05	4.33±0.07	267±4	0.425±0.010	9.13±0.06
7.52±0.04	4.36±0.15	269±9	0.419±0.020	9.16±0.12
7.59±0.03	4.39±0.12	273±8	0.422±0.016	9.19±0.10
7.43±0.03	4.45±0.08	271±5	0.401±0.011	9.22±0.06
7.73±0.03	4.57±0.10	289±6	0.409±0.013	9.35±0.08
8.17±0.06	4.61±0.09	309±6	0.435±0.012	9.43±0.07
7.92±0.05	4.66±0.11	303±7	0.412±0.014	9.44±0.09
8.36±0.06	4.75±0.08	325±6	0.433±0.010	9.56±0.06
8.51±0.08	4.92±0.05	343±4	0.422±0.008	9.71±0.04
8.48±0.03	5.08±0.11	354±8	0.400±0.013	9.85±0.09
8.80±0.04	5.20±0.09	376±7	0.409±0.010	9.98±0.07
8.92±0.06	5.35±0.12	391±9	0.400±0.014	10.11±0.10

^a Density is 0.820 g/cc.

the data and is

$$U_s = 1.17 \pm 0.17 + (1.72 \pm 0.06) U_p - (0.06 \pm 0.01) U_p^2 \quad (13)$$

There is fair agreement with the data of Walsh and Rice,⁸ and Cook and Rogers.⁹ For shock velocities between 3.50 and 4.75 km/sec Mitchell and Keeler²⁶ obtained a linear relationship which has a larger intercept and smaller slope than expressed by Eq. (11). The reason for this discrepancy is not known. The values of U_s for $U_p = 0$, as determined from Eqs. (11) and (13) are significantly larger than the measured sound speed. Bridgman⁵ found that the liquid freezes at a pressure of approximately 1 kbar at 25°C, which may account for the lack of agreement.

Figure 9 is a $P-V/V_0$ plot showing two concave upward curves corresponding to the two straight lines of Fig. 8. A slight cusp appears at about 164 kbar. A single curve through the data is equally descriptive, considering the quality of the data.

For shocked carbon tetrachloride, Walsh and Rice⁸ observed a slight change in transparency to visible light at about 70 kbar and complete opacity between 130 and 170 kbar. Previous dynamic pressure studies^{27,28} on carbon tetrachloride have found a large increase in electrical conductivity at pressures above 120 kbar. A thorough investigation by Mitchell and Keeler²⁶ revealed measurable conductivity at 69 kbar and very

high conductivity at 164 kbar. Hence, there seems to be a relation²⁹ between the onset of opacity and measurable electrical conductivity at about 70 kbar. In addition the opaqueness and the very high electrical conductivity observed in the 160–170-kbar range may also be related to the change in slope in the U_s-U_p plot at 164 kbar.

The observed behavior of carbon tetrachloride under shock conditions may be the result of the liquid polymerizing in the 70–170-kbar pressure range. The molecular rearrangement occurring in the polymerization process could free ions in sufficient quantity at 70 kbar to produce detectable changes in opacity and electrical conductivity. The change in slope of the U_s-U_p curve at 164 kbar may signal the end of this process, with the upper line corresponding to the new polymer. Based on some calculations³⁰ Mader of this laboratory has suggested that a different chemical species is formed according to the reaction $2\text{CCl}_4 \rightarrow \text{C}_2\text{Cl}_6 + 2\text{Cl}_2$ at pressures near 100 kbar while insignificant amounts of the new substance are formed below 50 kbar.

Another explanation for the change in slope of the U_s-U_p plot at 164 kbar is the following: A pressure-temperature graph of Bridgman's carbon tetrachloride freezing data³¹ and that from the Hugoniot information indicates that the Hugoniot curve crosses into a solid III phase at about 10 kbar. Then near 160 kbar the Hugoniot recrosses the liquid-solid phase

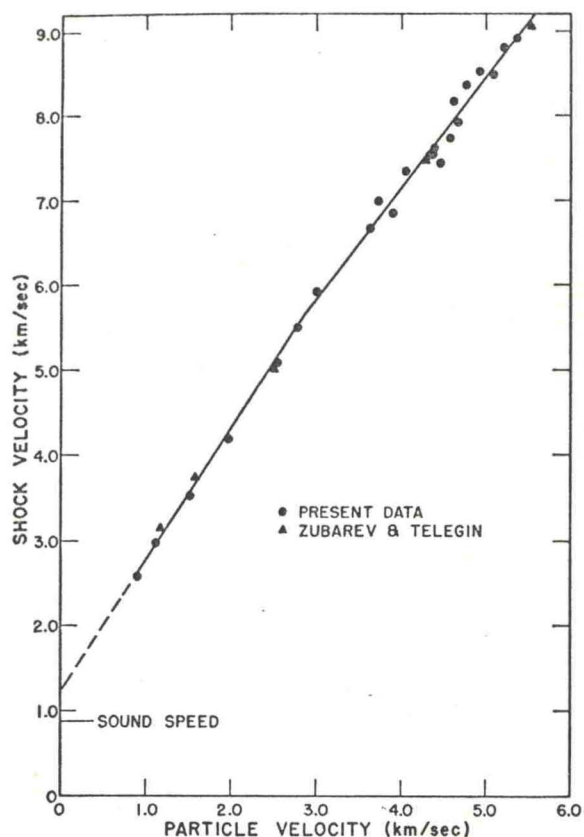


FIG. 10. Shock velocity-versus-particle velocity plot for liquid nitrogen.

line and remains in the liquid state. This particular explanation, however, does not explain the opacity and electrical conductivity changes observed at high pressures.

Temperatures for carbon tetrachloride shocked into

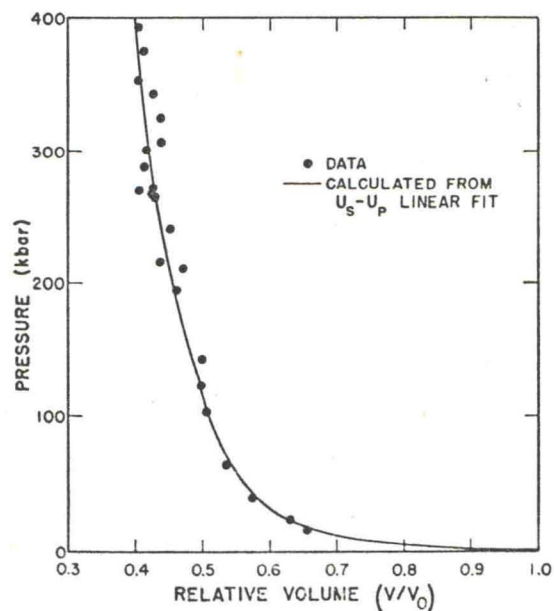


FIG. 11. Pressure-versus-relative volume plot for liquid nitrogen.

TABLE V. Potential parameters used for computing Hugoniot for liquid nitrogen.

Potential form (References)	r^* (Å)	T^* (°K)	n	α
LJD (present work)	4.17	97.5	9	...
LJD (Ref. 10)	4.19	91.5	12	...
LJD (Ref. 36)	4.16	95.9	7	...
LJD (Ref. 37) ^a	4.13	91.5	12	...
LJD (Ref. 35)	4.15	95.0	12	...
exp-6 (present work)	4.00	110.0	...	13.6
exp-6 (Ref. 34)	4.05	120.0	...	13.0

^a Gaseous nitrogen data.

the 70–170-kbar range were calculated to be between 1350 and 3500°K using the Mie–Grüneisen equation of state. Ramsey³² of this laboratory has measured a brightness temperature of 2400°K at 170 kbar. Recently, Voskoboinikov and Bogomolov³³ have reported measuring the brightness temperature of the shock front in carbon tetrachloride over a pressure range of 80–200 kbar. At 170 kbar they measured 2600°K.

A Hugoniot curve computed by Salzman, Collings, and Pings²² from a Lennard-Jones and Devonshire intermolecular potential is located slightly above the experimental Hugoniot curve when plotted in the

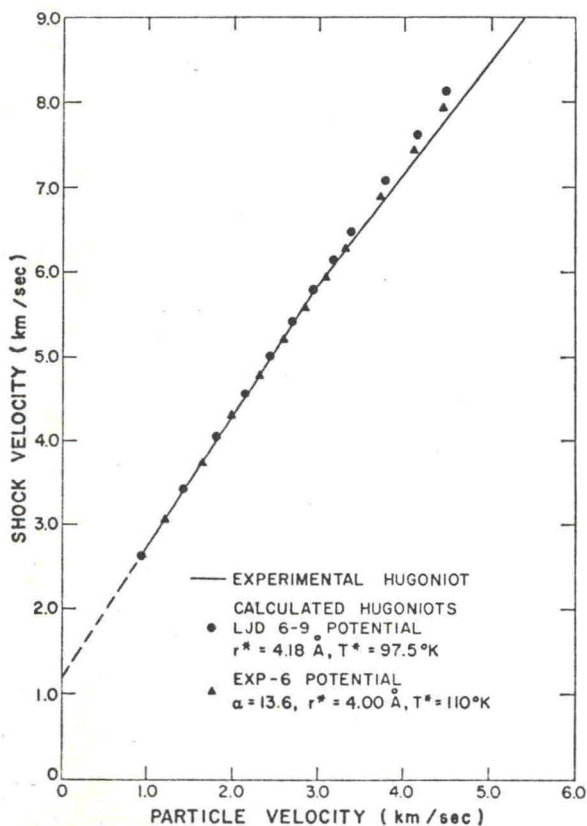


FIG. 12. Experimental and calculated Hugoniot for liquid nitrogen.

TABLE VI. Summary of results.

	Benzene	Carbon disulfide	Carbon tetrachloride		Liquid nitrogen	
Lower segment						
C (km/sec)	1.50 ± 0.10	1.18 ± 0.22	1.11 ± 0.08	1.17 ± 0.17	1.19 ± 0.06	1.12 ± 0.50
S	1.67 ± 0.04	1.67 ± 0.14	1.67 ± 0.05	1.72 ± 0.06	1.56 ± 0.03	1.68 ± 0.11
T (km/sec) ⁻¹	-0.06 ± 0.01	...	-0.04 ± 0.02
U_s limits (km/sec)	2.70-5.83	2.40-3.50	2.30-4.70	2.30-8.26	2.58-5.60	2.58-8.92
Middle segment		
C (km/sec)	4.64 ± 0.99	constant				
S	0.46 ± 0.10	shock				
T (km/sec) ⁻¹	...	velocity				
U_s limits (km/sec)	5.83-6.26	interval				
Upper segment			
C (km/sec)	1.37 ± 0.17	1.11 ± 0.07	1.87 ± 0.14		1.85 ± 0.38	
S	1.39 ± 0.03	1.35 ± 0.02	1.32 ± 0.03		1.32 ± 0.08	
T (km/sec) ⁻¹	
U_s limits (km/sec)	6.26-9.00	3.50-8.20	4.70-8.26		5.60-8.92	
Average initial temperature (°K)	293	293	293	293	75	75
Average initial density (g/cc)	0.879	1.264	1.594	1.594	0.820	0.820
Sound speed (km/sec)	1.31	1.16	0.93	0.93	0.88	0.88
Transition pressure (kbar)	133 ± 5	62 ± 4	164 ± 5	...	135 ± 3	...

U_s-U_p plane. An adjustment of the potential parameters ($n=6.4$, $r^*=6.60$ Å, and $T^*=327^\circ\text{K}$) would probably bring the two curves into better agreement.

E. Liquid Nitrogen

The Hugoniot data are presented in Table IV and in Figs. 10 and 11. The data reported by the Russian investigators¹⁰ are also included in the U_s-U_p plot. Since the initial temperature of the 2024 dural standard was the same as the liquid nitrogen, the equation of state of the 2024 dural had to be adjusted to 75°K , resulting in the equation,

$$U_s = 5.387 + 1.335U_p \quad (14)$$

with $\rho_0(75^\circ\text{K}) = 2.820$ g/cc and the Gruneisen ratio $\Gamma_0 = 2.0$.

The experimental assemblies were constructed and measured at room temperature. Distances and setbacks of pin contactors have been adjusted to allow for the thermal contraction to 75°K . The values listed in Table IV for the shock velocities reflect this adjustment.

Two straight lines fit the U_s-U_p data with a change in slope occurring at about $U_s = 5.60$ and $U_p = 2.90$ km/sec. The lower line fits

$$U_s = 1.19 \pm 0.06 + (1.56 \pm 0.03)U_p \quad (15)$$

and the upper line fits

$$U_s = 1.85 \pm 0.38 + (1.32 \pm 0.08)U_p \quad (16)$$

A smooth curve also provides a good fit of the data

and is described by a quadratic in U_p ,

$$U_s = 1.12 \pm 0.50 + (1.68 \pm 0.11)U_p - (0.04 \pm 0.02)U_p^2 \quad (17)$$

The present data agree reasonably well with the Russian results.

The intercept with the U_s axis defined by Eq. (15) is higher by nearly 35% than the reported sound speed³⁴ of 0.88 km/sec. This leads to the possibility of a transition occurring below 19 kbar, the lowest pressure used in this study.

The $P-V/V_0$ plot of Fig. 11 shows two concave upward curves with a cusp at 135 kbar. There is considerable scatter of the points, especially at the higher pressures. A temperature associated with 135-kbar pressure was calculated to be 3400°K . If a transition occurs at this pressure, the Hugoniot could cross into the solid phase below 19 kbar and then at 135 kbar recross the fusion line and remain in the solid-liquid mixed-phase region.

Liquid nitrogen shock Hugoniot have been calculated^{35,36} using a Lennard-Jones and Devonshire and a modified Buckingham (exp-6) intermolecular potential which agree well with the experimental Hugoniot between 20 and 170 kbar. The calculations were performed with a computer code developed by Fickett of this laboratory. The code is based on the cell model and assumes: The pair potentials are additive; each cell has 12 nearest neighbors; there is one molecule per cell. The 12 nearest neighbors are uniformly smeared over a spherical surface whose radius cor-

responds to the nearest-neighbor distance. The calculated Hugoniot which agree with the experimental Hugoniot have the following potential forms:

$$\text{LJD } \Phi(r) = [kT^*/(n-6)] [6(r/r^*)^{-n} - n(r/r^*)^{-6}], \quad (18)$$

$$\text{exp-6 } \Phi(r) = [kT^*/(\alpha-6)] \times \{6 \exp[\alpha(1-r/r^*)] - \alpha(r/r^*)^{-6}\}, \quad (19)$$

where r^* is the position of the potential minimum, T^* is the temperature equivalent of the energy of the potential minimum at $r=r^*$, r is the intermolecular distance, k is Boltzmann's constant, n is the repulsion term for the LJD form, and α is the steepness parameter for the exp-6 form. Table V is a list of the values for these "constants" from which the Hugoniot were calculated. Also included for comparison are the values used by others. Figure 12 shows the calculated and experimental Hugoniot. The most recent calculations²² are by Salzman, Collings, and Pings. These agree with the experimental Hugoniot and the parameters used except for the value of n in the repulsion term. A comparison of the parameters for the exp-6 potential used in this study with Fickett's values indicated close agreement. No significance was placed on the separation of the experimental and calculated Hugoniot curves about 170 kbar. The calculated Hugoniot indicates a stiffer material than observed.

IV. SUMMARY

Table VI summarizes the equation of state parameters obtained for each liquid and indicates the appropriate range, standard deviations, and initial conditions. The benzene and carbon disulfide U_s-U_p data are represented by a linear relationship while the carbon tetrachloride and liquid nitrogen data are represented equally well by a linear relationship or by a quadratic in U_p . A transition occurs in benzene and carbon disulfide with the possibility of a mixed phase region existing between the low and high pressure phases. The evidence for the occurrence of a transition in carbon tetrachloride and liquid nitrogen is not as strong as for the other two liquids. Considering Table VI, the values for the slope of the lower and upper line segments for each liquid are very similar.

ACKNOWLEDGMENTS

The author acknowledges the technical assistance of T. E. Gould in constructing and firing the experimental assemblies and the helpful discussions with W. E. Deal and R. H. Warnes. S. Landeen provided assistance in preparing this manuscript.

* Submitted to Arizona State University April 1968 in partial fulfillment of the requirements for the Ph.D. degree.

† This work was performed under the auspices of the U.S. Atomic Energy Commission.

¹ P. W. Bridgman, Proc. Am. Acad. Arts Sci. 49, 3 (1913).

² P. W. Bridgman, Proc. Am. Acad. Arts Sci. 66, 185 (1931).

³ P. W. Bridgman, J. Chem. Phys. 9, 794 (1941).

⁴ P. W. Bridgman, Proc. Am. Acad. Arts Sci. 74, 399 (1942).

⁵ P. W. Bridgman, Proc. Am. Acad. Arts Sci. 77, 129 (1949).

⁶ P. W. Bridgman, Phys. Rev. 46, 930 (1934).

⁷ P. W. Bridgman, Proc. Am. Acad. Arts Sci. 70, 1 (1935).

⁸ J. M. Walsh and M. H. Rice, J. Chem. Phys. 26, 815 (1957).

⁹ M. A. Cook and L. A. Rogers, J. Appl. Phys. 34, 2330 (1963).

¹⁰ V. N. Zubarev and G. S. Telegin, Dokl. Akad. Nauk SSSR

142, 309 (1962) [Sov. Phys. Dokl. 7, 34 (1962)].

¹¹ M. H. Rice, J. M. Walsh, and R. G. McQueen, Solid State

Phys. 6, 1 (1958).

¹² W. E. Deal, Jr., in *Modern Very High Pressure Techniques*, edited by R. H. Wentorf, Jr. (Butterworth, Washington, D.C., 1962), Chap. 11.

¹³ G. E. Duvall and G. R. Fowles, in *High Pressure Physics and Chemistry*, edited by R. S. Bradley (Academic, New York, 1963), Vol. 2, Chap. 9.

¹⁴ W. J. Carter, S. P. Marsh, J. N. Fritz, and R. G. McQueen, "The Equation of State of Selected Materials for High Pressure References," Los Alamos Scientific Lab. Rept. LA-DC-9990, 1968.

¹⁵ R. D. Dick, "Shock Wave Compression of Benzene, Carbon Disulfide, Carbon Tetrachloride, and Liquid Nitrogen," Los Alamos Scientific Lab. Rept. LA-3915; available from Clearinghouse for Federal Scientific and Technical Information, National Bureau of Standards, U.S. Department of Commerce, Springfield, Va. 22151; printed copy \$3.00, microfiche \$0.65.

¹⁶ R. D. Dick and T. E. Gould, Rev. Sci. Instr. 36, 143 (1965).

¹⁷ R. G. McQueen, in *Metallurgy at High Pressures and High Temperatures*, edited by K. A. Gschneidner, Jr., M. T. Hepworth, and N. D. Parlee (Gordon and Breach, New York, 1964), pp. 44-132.

¹⁸ R. G. McQueen, S. P. Marsh, and J. N. Fritz, J. Geophys. Res. 72, 4999 (1967).

¹⁹ R. Ford of this laboratory measured the sound speeds of benzene, carbon disulfide, and carbon tetrachloride at 22°C and local atmospheric pressure and found the speeds to be 1.31, 1.16, and 0.93 km/sec, respectively.

²⁰ R. H. Warnes, J. Appl. Phys. 38, 4629 (1967).

²¹ R. H. Warnes, Bull. Am. Phys. Soc. 13, 579 (1968).

²² P. K. Salzman, A. F. Collings, and C. J. Pings, J. Chem. Phys. 50, 935 (1969).

²³ E. Whalley, Can. J. Chem. 38, 2105 (1960).

²⁴ E. G. Butcher, M. Alsop, J. A. Weston, and H. A. Gebbie, Nature 199, 756 (1963).

²⁵ A. S. Kusubov (private communication).

²⁶ A. C. Mitchell and R. N. Keeler, Rev. Sci. Instr. 39, 513 (1968).

²⁷ D. G. Doran and T. J. Ahrens, "Electrical Effects of Shock Waves," Stanford Research Institute Final Report PGU-4100, 1963.

²⁸ R. D. Dick, Bull. Am. Phys. Soc. 9, 547 (1964).

²⁹ S. D. Hamann, in *Advances in High Pressure Research*, edited by R. S. Bradley (Academic, New York, 1966), Vol. 1, Chap. 2.

³⁰ C. Mader (private communication).

³¹ P. W. Bridgman, Phys. Rev. 3, 126 (1914).

³² J. Ramsey (private communication).

³³ I. M. Voskovoinikov and V. M. Bogomolov ZhETF Pis. Red. 7, 338 (1968) [JETP Letters 7, 264 (1968)].

³⁴ A. Van Itterbeck and W. Van Dael, Physica 28, 861 (1962).

³⁵ W. Fickett, "Detonation Properties of Condensed Explosives Calculated with an Equation of State Based on Intermolecular Potentials," Los Alamos Scientific Lab. Rept. LA-2712, 1962.

³⁶ W. Fickett, "Intermolecular Potential Functions for Some Simple Molecules from Available Experimental Data," Los Alamos Scientific Lab. Rept. LA-2665, 1962.

021000 08202

LA-DC